Smart Structures and Systems, *Vol. 27, No. 1 (2021) 89-99*
DOI: https://doi.org/10.12989/sss.2021.27.1.089

An innovative liquid metal-based pressure sensor with its application in geotechnical engineering

Yundong Shou [1], Xiaoping Zhou*[1,2], Qingpeng Chang [2] and Chao Liu [2]

[1] *School of Civil Engineering, Wuhan University, Wuhan 430072, China*
[2] *School of Civil Engineering, Chongqing University, Chongqing 400045, China*

(*Received April 5, 2020, Revised July 4, 2020, Accepted July 6, 2020*)

Abstract. In this paper, a monitoring system containing a novel liquid metal-based pressure sensor and remote interactive monitoring devices are fabricated to monitor stress in geotechnical engineering. The pressure sensor with the dimension of 34 mm × 34 mm is designed and manufactured, which is mainly composed of 40CrMoV alloy steel shell, polydimethylsiloxane (PDMS) and liquid metal gallium indium alloy (EGaIn). It has the characteristics of high stability, can greatly improve the measurement range of the pressure sensor (0 to 20 MPa), and its resistance variation is from 0 mΩ to 800 mΩ. In addition, the linear regression analysis is carried out to verify the linear relationship between the resistance of sensor and the applied pressure. It is found that the performance of the pressure sensor is fine through experiments with three different loading rates and fatigue experiments. The remote interactive monitoring device can be suitable for the field monitoring environment, which is composed of monitoring stations (MS), remote communication base stations (RCBS) and indoor working platform. Finally, the monitoring system is successfully applied to the field measurements in geotechnical engineering, and the field monitoring data are in good agreement with the numerical results.

Keywords: geotechnical engineering; pressure sensor; polydimethylsiloxane (PDMS); liquid metal; field monitoring

1. Introduction

In geotechnical engineering, the most of engineering accidents are mainly attributed to the deterioration of geological conditions and structural instability, so the engineering monitoring is receiving more and more attention. To obtain stress distribution information of rock-soil mass and supporting system is very important for studying stability of geotechnical engineering, such as slope, underground, foundation, bridge and tunnel engineering (Holtz *et al*. 2010, Kou *et al*. 2019). Pressure sensor plays a key role in monitoring the stress of rock-soil mass and supporting system, and it is used as an important technology for long-term monitoring in combination with other transmission equipment. Therefore, many different pressure sensors are developed, such as resistance pressure sensor, piezoresistive pressure sensor, piezoelectric pressure sensor, capacitance pressure sensor, fiber optic pressure sensor, distributed optical fiber pressure sensor, and so on.

Generally, the most widely used is resistance sensor, which is based on the principle of strain-resistance effect. The resistive pressure sensors, which are composed of the elastic element and sensitive element, can be divided into two types according to the structure of pressure sensor. The first type is to integrate the elastic element and sensitive element together as the elastic-sensitive element, which is usually the silicon chip, such as the silicon-on-insulator (SOI) pressure sensors (Kurtz *et al*. 2003, Kurtz *et al*. 2004, Zhao *et al*. 2006). Moreover, the measuring range of the first type of pressure sensors is determined by the structure of the silicon chip and silicon material, and it would have a fine accuracy when the pressure measured is less than 100 MPa (Zhao *et al*. 2013). The second type of pressure sensors is to package the sensitive elements on the elastic elements, such as silicon-on-sapphire (SOS) pressure sensor (Stuchebnikov 1991, Zhang *et al*. 2001), sputtered thin film pressure sensor (Raiendra *et al*. 2005, Yan *et al*. 2005), strain gauge pressure sensor (Orhan *et al*. 2001), etc. However, almost all of these sensors are made of brittle solid materials, which are prone to fatigue and brittle failure under cyclic loads. And also, there are many reports of piezoresistive flexible pressure sensors (Chen *et al*. 2017, Wang *et al*. 2014, Jia *et al*. 2019, Zhang *et al*. 2017, 2019, Ryu *et al*. 2011, Chuang *et al*. 2012), but most piezoresistive devices have narrow detection ranges. For low pressure measurements, the piezoresistive pressure sensor has a new structure in Li *et al*. (2017), and improves the sensitivity in Yu *et al*. (2013), Yu and Huang (2015). Moreover, the structure of piezoresistive sensor plays a key role in the performance of the piezoresistive sensor. Based on the film geometry and varistor size, the performance of silicon piezoresistive pressure sensor (Nisanth *et al*. 2014a) and the sensitivity of silicon-based MEMS pressure sensor (Nisanth *et al*. 2014b) have been studied. Some scholars have analyzed the dynamic performance of micro pressure sensor (Tian *et al*. 2014). The performance and energy efficiency of wireless sensing system for pressure

*Corresponding author, Professor,
E-mail: cqxpzhou@hotmail.com

ISSN: 1738-1584 (Print), 1738-1991 (Online)

monitoring have also been investigated by some researchers (Cui *et al*. 2007, Xu *et al*. 2015).

In addition, a flexible piezoelectric pressure sensor (Signore *et al*. 2018) is developed based on AlN, but it cannot measure large pressures. More and more attention has been paid to new capacitive pressure sensors with large dynamic range (Bakhoum and Cheng 2010a, b), but they cannot be directly applied to geotechnical engineering. At the same time, many scholars make use of the characteristics of optical fiber to make optical fiber pressure sensor (Vorathin *et al*. 2020, Wang *et al*. 2019). At present, distributed fiber optic sensing has been recognized as one of the potential technologies that could revolutionize structural and geotechnical monitoring (Klar *et al*. 2016, Barrias *et al*. 2016, Soga and Luo 2018, Gue *et al*. 2014, Minardo *et al*. 2018). However, the bare optical fiber is fragile and is prone to break in the actual monitoring process.

Recent years, engineering monitoring is mainly based on instrument measurement and record, which is gradually developed to intelligent monitoring and early warning of automatic control. Manual or semi-automatic monitoring has obvious time domain blank, poor real-time performance, and it is difficult to achieve basic data collection under adverse conditions such as night and rainy days. The reliability of data collection is greatly affected by external environmental factors, so it is difficult to meet the needs of automatic real-time monitoring. Although the existing automatic monitoring system includes sensing, acquisition, transmission, power supply, lightning protection, installation accessories and other parts, it is difficult and complicated to implement in the geotechnical engineering due to their relatively low integration. The advanced geotechnical engineering construction technologies, such as the TBM construction method, have put forward higher request on automatic monitoring system (Haeri and Marji 2016, Haeri *et al*. 2013, 2016, Sarfarazi *et al*. 2017, Sarfarazi *et al*. 2019). Therefore, it is necessary to the integration design of multi system components, which provides great convenience for site installation and maintenance.

Based on the above, the pressure sensors with flexibility, large pressure range and highly integrated remote monitoring equipment need to be fabricated to monitor stress in geotechnical engineering. Because of the good electrical performance and fluidity of gallium indium (Ga-In) liquid metal, it was increasingly used in the measurement of large deformation (Kim *et al*. 2019). Chossat *et al*. (2013) developed a soft strain sensor which have the capable of withstanding strains of up to 100%. Ali *et al*. (2016a, b) described a flexible pressure sensor with Polydimethylsiloxane (PDMS) and EG-In based liquid metal, and the measurement range of the flexible pressure sensor is from 0.25 MPa to 1.1 MPa. Oh *et al*. (2019) presented a pressure-conductive rubber sensor using a liquid-metal-polydimethylsiloxane. The sensor can operate reliably under various elastic deformations such as pressing, stretching, and bending without structural failure and performance degradation. In this paper, we have made some optimization in size and improved measuring range of the liquid metal pressure sensor compared with previous studies. The output signal stability of pressure sensor was evaluated at different loading rates. Moreover, the remote interactive monitoring device integrating the multi system components combines with the pressure sensor to form a complete geotechnical engineering monitoring system and to make field measurements in the actual tunnel engineering. In addition, the field monitoring data are compared with the numerical results. Most importantly, the purpose of long-distance, long-term and real-time acquisition of the stress of the monitoring target is realized by pressure sensor and remote interactive monitoring system.

2. Fabrication and theory

2.1 Fabrication

The completed monitoring system includes liquid metal pressure sensor and remote interactive monitoring device, as shown in Fig. 1. In addition, the remote interactive monitoring device include monitoring stations (MS), remote communication base stations (RCBS) and indoor working platform. The MS can simultaneously connect four pressure sensors through silver-plated wires, and the transmission of electrical signals (change of resistance) between RCBS and MS is carried out by wireless, as well as the transmission between RCBS and indoor working platform, as shown in Fig. 1.

2.1.1 Fabrication of pressure sensor

The pressure sensor is consisted of steel case and prototype, in which the prototype is encapsulated in the steel shell. The working principle of the liquid metal pressure sensor designed in this paper is described as follows: the PDMS microfluidic prototype is used as the sensitive element of pressure sensor, in which a microchannel is filled with liquid metal (EGaIn); the cross-sectional area of micro-channel is changed when the PDMS microfluidic prototype is subjected to stress; the resistance of liquid metal of pressure sensor increases with decreasing its cross-sectional area. Therefore, the liquid metal pressure

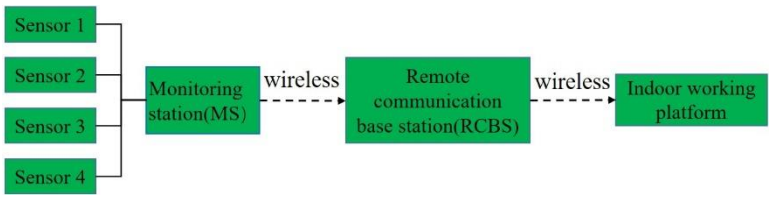

Fig. 1 The completed monitoring system

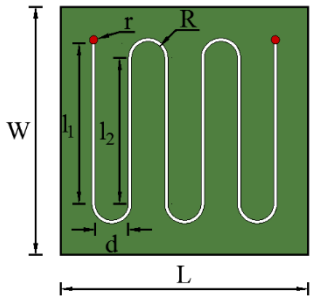

Fig. 2 Micro-channels of sensor prototype

sensor can be used to obtain the external pressure through the change of resistance.

As shown in Fig. 2, the micro-channel in PDMS prototype is S-shaped, which reduces the obstruction of liquid metals to flow under the applied pressure. The cross-sectional dimension of the micro-channels and the spacing between them are shown in Table 1. It is worth noting that the smaller the cross-section size of the micro-channel, the greater the resistance of the sensor, the greater the resistance changes with the pressure, and the higher the sensitivity of the sensor. The size and layout of microchannel designed can well meet the requirements of small size and large range of pressure sensor. Before the micro-channels are made, the stress distribution around the micro-channels under the external pressure is simulated by using the finite element method. It is found that the stress near the micro-channel is relatively large, which makes the micro-channel deform greatly under the applied pressure, so that the resistance of the liquid metal changes obviously.

The PDMS elastomer prototype was fabrication by using soft lithography technique (Zhou *et al*. 2018, 2019), which is a mature micro-fabrication strategy. To make the sensor prototype, we need two moulds and PDMS material with a ratio of base liquid to curing agent of 10:1. The fabrication procedure of the sensor prototype is described briefly as follows:

(1) The moulds with micro-channels are fabricated based on the designed size of the sensor shown in Fig. 2. The surface of moulds is treated, as shown in Figs. 3(a)-(b).
(2) The liquid PDMS and curing solution were mixed in a ratio of 10:1 into the container and stirred evenly. The uniformly mixed solution is put into a vacuum oven to remove air bubbles generated during the stirring process.
(3) When air bubbles are removed, the PDMS mixture is poured into the mould in a petri dish, then the petri dish with the mould is put on a heating table at 80°C to cure. After approximately half an hour of heating, the PDMS is completely solidified, as shown in Fig. 3(c).
(4) The PDMS is demolded from the mould, and is cut to the designed substrate size. Next, two endpoints of microfluidic channels are punched with

Table 1 The design parameters for the sensor prototype

Design parameters of micro-channel	Symbol	Value (mm)
Radius of inlet and outlet of channel	r	0.5
Channel width	w	0.4
Channel height	h	0.2
Length of lateral channel	l_1	19.8
Length of inner channel	l_2	17.6
Distance between adjacent two channels	d	4
Inner radius of curved channel	R	4
Channel depth	h_t	4.9

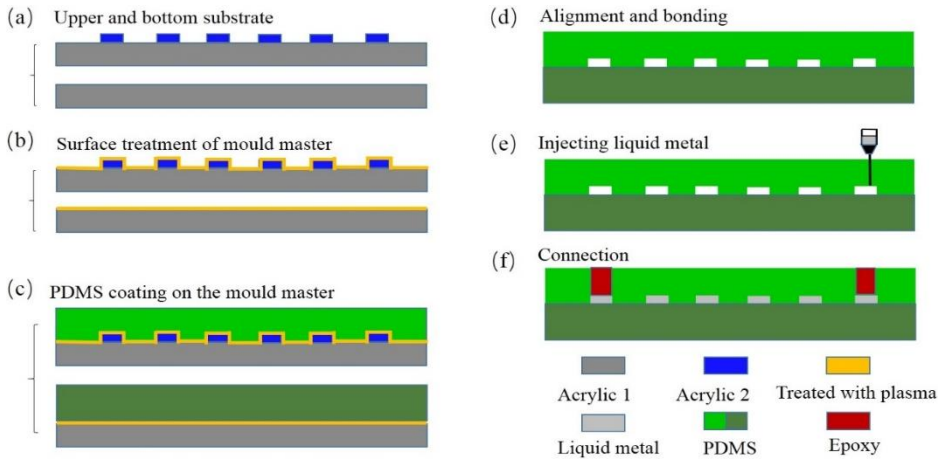

Fig. 3 Detailed fabrication steps of sensor prototype

a stainless-steel TiN-coated round punch with the dimension of 0.2 mm × 1 mm (Technical Innovations, Angleton, TX) to create through-holes that serve as the inlets and outlets for the injection of liquid metal, as shown in Fig. 3(d).

(5) The cleaned glass chip and the PDMS chip are treated with plasma and removed after 30 s, then the PDMS and the glass chips are aligned based on the designed substrate size, the production of the PDMS chip is completed, as shown in Figs. 3(c)-(d).

(6) After the PDMS prototype with microchannel is fabricated, the liquid metal EGaIn is injected into the micro-channel through using a syringe, as shown in Fig. 3(e).

(7) When the inlet and outlet are sealed by epoxy, the manufacture of a liquid-metal sensor prototype is complete, as shown in Fig. 3(f).

The complete prototype before injecting liquid metal and after injecting liquid metal were shown in Figs. 4(a)-(b), respectively.

To detect the stress in geotechnical engineering, the 40CrMoV alloy steel shell, which matches the size of the elastomer, is installed on the elastomer, as shown in Fig. 5. The 40CrMoV alloy steel has high strength and low hysteresis elasticity (Zhou *et al*. 2018, 2019, Berto *et al*. 2014, Park *et al*. 2012), which also greatly improves the measurement range of pressure sensor and ensures the stability and reliability of test results. The 40CrMoV alloy steel shell is made strictly based on the size of the matching elastomer through finishing technology.

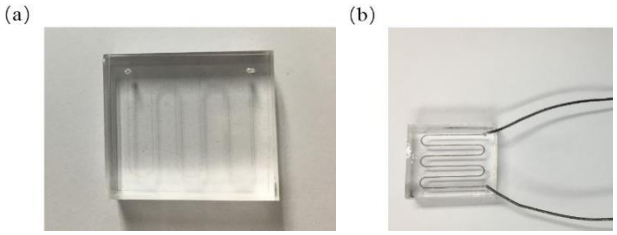

Fig. 4 Complete sensor prototype: (a) Samples after bonding; (b) Samples injected with liquid metal and wires

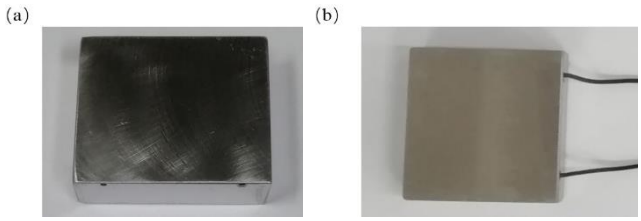

Fig. 5 The 40CrMoV metal shell (a) and complete pressure sensor (b)

2.1.2 Theory of pressure sensor

When the pressure is applied to the sensor, the elastomer prototype is subject to pressure of P shown in Fig. 6. Then, the cross section of the micro-channel is deformed by the applied pressure, which changes the resistance of the liquid metal of the micro-channel. Under pressure of P, the cross-section area of rectangular micro-channel becomes (Zhou *et al*. 2018)

$$A_f = w\left[h - \frac{2(1-v^2)pw}{E}\right] \tag{1}$$

where, w and h are respectively the width and height of the rectangular cross section of the micro-channel, v and E are Poisson's ratio and Young's modulus of the PDMS, respectively.

According to Ohm's Law $R = \rho L/A$, the change of resistance (ΔR) is

$$\Delta R = \rho L\left(\frac{1}{A_f} - \frac{1}{A_0}\right) \tag{2}$$

where, ρ is the resistivity of liquid metals, L and A are respectively the length and cross-sectional area of micro-channel with liquid metal, the subscripts f and 0 represent the cross-sectional area after pressure is applied and in the initial state, respectively.

2.2 Composition of remote interactive monitoring device

As a necessary instrument for collecting and transmitting sensor signals, the remote interactive monitoring device plays a key role in the realization of remote real-time monitoring in geotechnical engineering. The MS and RCBS are important components of remote interactive monitoring, their functions need to meet the requires of remote multi-point real-time monitoring. The MS can be connected with four sensors simultaneously by wire, as shown in Fig. 7. Moreover, the MS collects and processes the monitoring pressure signals into electrical signals, and it also transmits electrical signals to the RCBS by wireless transmission. Then, the RCBS transmits the electrical signal to the indoor working platform remotely for monitoring, which can realize the remote real-time monitoring in geotechnical engineering.

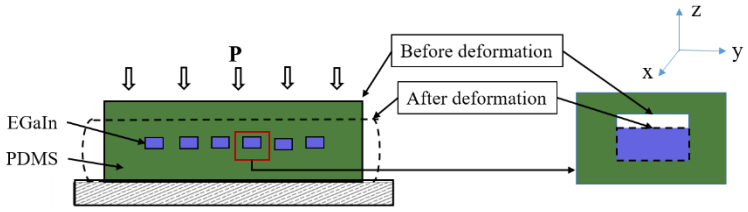

Fig. 6 Principle sketch of deformation after loading

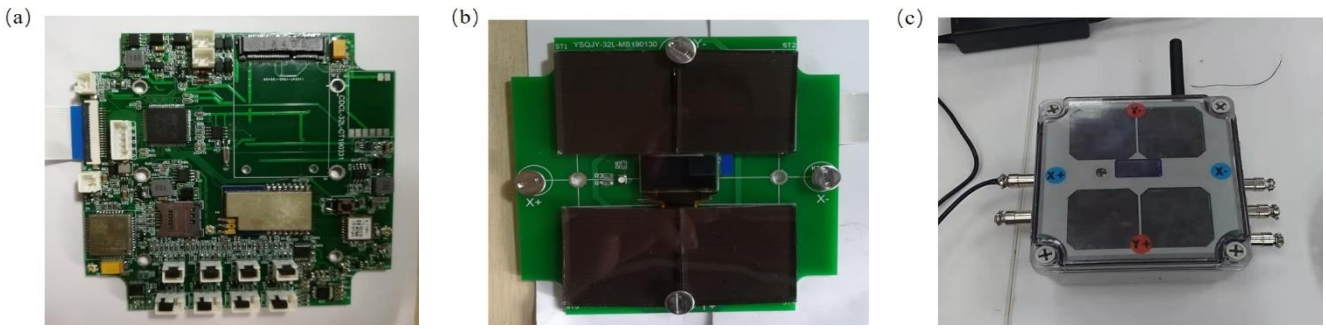

Fig. 7 Components of the monitoring station (MS). (a) PCB circuit board; (b) micro solar panel; and (c) complete monitoring station after assembly

To achieve above functions, the MS is integrated by a signal acquisition module, a signal processing module, an early warning driving module, a communication module and a display module. The advantage is to make the installation and deployment of MS more convenient. Similarly, the RCBS is also integrated by multiple system components, which includes ultra-low power management, ad hoc network module, Beidou short message, GNSS positioning, solar energy, NBIOT communication module, temperature-humidity environment monitoring module, embedded CPU and multi task embedded operating system. Because these functional modules are used in the interactive monitoring system, the remote real-time monitoring of multiple points can be realized.

3. Calibration experiments of the pressure sensor

As the most important part of the whole monitoring system, the working principle of liquid metal pressure sensor is applied to obtain the external pressure by measuring the resistance change of the sensor. Before the pressure sensor is applied to engineering practice, it is necessary to calibrate the pressure sensor to obtain the relation between sensor resistance and external pressure.

3.1 The equipment required for calibration experiments

In the calibration experiments, CMT 5504 Universal Mechanical Testing Machine shown in Fig. 8, and DC Resistance Tester shown in Fig. 9 are used to study the performance of pressure sensor. In all the experiments, the loading mode is controlled by forces.

The DC resistance tester with maximum resolution of 0.1 mΩ is used to measures resistance of pressure sensor in the calibration experiments. Before measuring resistance of sensor, the required range of the DC resistance meter should be chosen, and the display resistance should be adjusted to zero by connecting two test lines after waiting for 20 minutes of preheating in the boot state.

3.2 Calibration experiment result analysis of pressure sensor

In order to ensure the repeatability and accuracy of the test results of pressure sensor, the experimental results were taken by the average value through multiple loading with loading rate of 0.05kN/s. During the process of analysis, the variation of the resistance (ΔR) of pressure sensor is regarded as the object of analysis rather than the resistance (R), which can eliminate the influence on the fitting equation due to the different initial value of the resistance caused by the fabrication process.

The calibration experiment results show that there is an obvious linear correlation between the resistance change of the sensor and the applied external pressure, as shown in Fig. 10. When linear fitting is performed, the resistance variation (ΔR) of the pressure sensor is defined as an independent variable, while the pressure (P) is defined as a dependent variable. The reliability of the regression straight line of the sample are evaluated by R test with a significance level of $\alpha = 0.01$ in statistics.

Fig. 8 CMT 5504 Universal Mechanical Testing Machine

Fig. 9 DC Resistance Tester

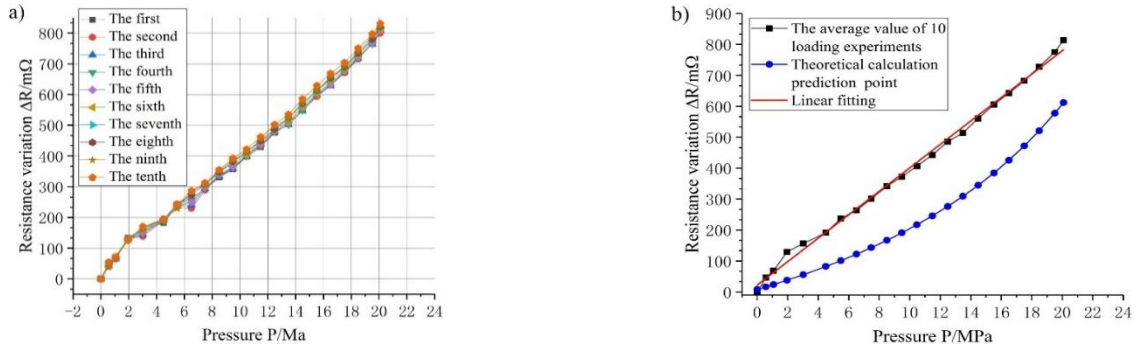

Fig. 10 The calibration experiment results. (a) pressure-resistance curves of ten groups under the repeated loading; and (b) the fitting line and theoretical calculation

Before the linear fitting and significance test, it is supposed that the linear regression equation of one variable can be written as

$$P = \beta_0 + \beta_1 \Delta R \tag{3}$$

where β_0 and β_1 are regression coefficients in the regression equation.

The estimated values $\widehat{\beta_0}$ and $\widehat{\beta_1}$ of regression coefficients are calculated by least square estimation, and the calculation equation can be written as follows

$$\widehat{\beta_1} = \frac{\sum_{i=1}^{n}(\Delta R_i - \overline{\Delta R})\,(P_i - \bar{P})}{\sum_{i=1}^{n}(\Delta R_i - \overline{\Delta R})^2} \tag{4}$$

$$\widehat{\beta_0} = \bar{P} - \widehat{\beta_1}\overline{\Delta R} \tag{5}$$

where, n is the number of experimental data points, $\overline{\Delta R}$ and $\bar{P}$ are the average values of ΔR and P, respectively.

According to the results of pressure sensor obtained by repeated loading experiments, the parameters of sample regression straight line can be calculated, and the results are listed in Table 2.

The fitting equation, in which the pressure value P (MPa) changes with the resistance change ΔR (mΩ) of the sensor, is $\hat{P} = 0.0263\Delta R - 0.5455$.

There is a deviation between the theoretical value and the experimental value, as shown in Fig. 10(b). The reason for this deviation may be that the deformation of the microchannel in the y-axis direction is ignored. The theoretical change of cross-section area of micro-channel is smaller than the real change, so the experimental data are larger than the theoretical results. Although there exists the deviation, we get a good linear relationship between the resistance change and the pressure during the repeated experiments.

Table 2 The parameters of sample regression line

$\overline{\Delta R}$	$\bar{P}$	$\widehat{\beta_1}$	$\widehat{\beta_0}$
398.4709	9.9383	0.02631	-0.54547

3.3 The stability of pressure sensor

As a signal acquisition device, the liquid metal pressure sensor in this paper is mainly applied to obtain the internal stress in rock-soil mass and the stress exerted on the supporting system in geotechnical engineering. The pressure sensors are often required to be buried in rock-soil mass for a long time in the practical application process. Therefore, the pressure sensor should have good stability to continuously and accurately monitor the stress of monitoring target.

In the calibration experiment, the deviation degree of resistance variation (ΔR) under the same pressure is also an important parameter to evaluate the stability of the sensor. We define the degree of signal deviation (ε) to further judge the stability of the sensor. The independent and dependent variables of Eq. (3) are exchanged to obtain another expression of the fitting equation, that is

$$\widehat{\Delta R} = 37.879P + 22.019 \tag{6}$$

The deviation degree ε can be defined as

$$\varepsilon = \frac{\left|\Delta R_i - \Delta \widehat{R_i}\right|}{\Delta \widehat{R_i}} \tag{7}$$

where, ΔR_i is the resistance change of the actual output of the sensor, and $\Delta \widehat{R_i}$ is the resistance change of the pressure sensor calculated from Eq. (6).

We calculate the deviation (ε) of sample points at loading rate of 0.05 kN/s, and all sample points are divided into six levels based on the deviation degree (ε): $\varepsilon < 1\%, 1\% \le \varepsilon < 2\%$ $2\% \le \varepsilon < 3\%, 3\% \le \varepsilon < 4\%, 4\% \le \varepsilon < 5\%,$ and $\varepsilon \ge 5\%$. The statistical results of each level are shown in Table 3.

The deviation degree of $\varepsilon < 5\%$ accounts for 89.55% of all samples in calibration experiments. It can be

Table 3 Deviation of sensor signal output at loading rate of 0.05 kN/s

$\varepsilon < 1\%$	$1\% \le \varepsilon < 2\%$	$2\% \le \varepsilon < 3\%$	$3\% \le \varepsilon < 4\%$	$4\% \le \varepsilon < 5\%$	$\varepsilon \ge 5\%$
30%	27.73%	18.64%	8.18%	5%	10.45%

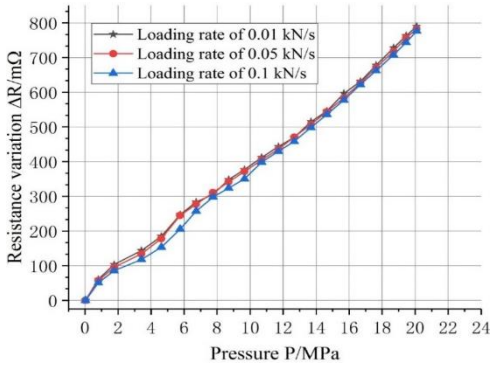

Fig. 11 Pressure-resistance curve under different loading rates

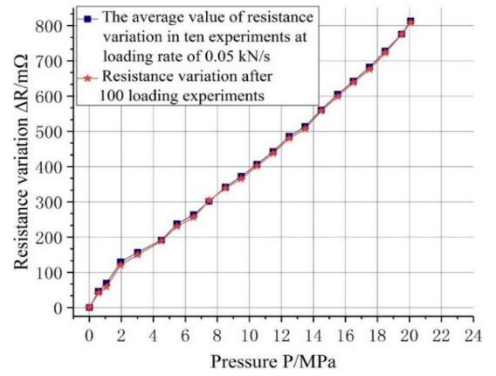

Fig. 12 The pressure-resistance curve after 100 loading experiments and calibration experiments

concluded that the signal output of pressure sensor is stable at loading rate of 0.05 kN/s.

Moreover, in order to investigate the influence of loading rate on the output stability of the pressure sensor, three different loading rates (0.01 kN/s, 0.05 kN/s and 0.1 kN/s) were implemented in the calibration experiments. To ensure the reliability of the experimental results, the pressure sensor is loaded three times at each loading rate. The experimental results at three loading rates are shown in Fig. 11. It can be found from Fig. 11 that the resistance variation (ΔR) changes slightly with increasing the loading rate and the measurement range of the sensor is improved to 20 MPa.

In addition, the sensor is repeatedly loaded 100 times to study the influence of multiple loading fatigue on the stability of the sensor. The results subjected to multiple loading fatigue highly match the calibration experiment results, as shown in Fig. 12. The deviation degree of $\varepsilon \geq 5\%$ accounts for 13.63%. It is found that the sensor has good stability at different loading rates and multiple loading fatigue. Of course, the factors that affect the stability of the sensor are not only mentioned above, other factors will be studied in the future works.

4. Field measurements and numerical simulations

4.1 Performance and installation of monitoring device

In the field measurement, the equipment performance determines whether the remote automatic monitoring can be realized or not, especially in the power supply and wireless transmission. In the MS and RCBS, solar panels are installed to realize self-power supply. Without external power supply, the MS and RCBS can continuously work for 5-7 years through the solar panel function as long as they have enough 24-hour sunshine every month. When the solar energy fails and there is no external power supply at the same time, the MS and the RCBS can respectively work for one year and one month only with the internal integrated battery. The signal acquisition frequency of the MS can be set or modified through remote workbench. The memory cards of both the above devices are a standard 8G, which can ensure that the signal data can be collected and stored at the frequency of once per minute for more than 8 years. However, the field measurement is carried out in the tunnel, and the solar panel function of the MS cannot be used. Therefore, the MS device adopts 220 V external DC power supply in Tiefeng tunnel, and the RCBS is self-powered by solar panels outside the tunnel.

The geomorphological map of Tiefeng mountain is shown in Fig. 13. The tunnel project is located in Tiefeng mountain area between Tiancheng, Wanzhou and Changsha town, Kaixian in Chongqing. The axial line of the tunnel is nearly orthogonal to the axial line of anticline of Tiefeng mountain, and the tunnel passes through the whole Tiefeng mountain. The elevation of the Tiefeng tunnel entrance is 310.55 m, and the elevation of Tiefeng tunnel exit is 427.29 m. The highest elevation in the tunnel site is 1286.00 m, and the maximum buried depth of the tunnel is 858.2 m. The north of Tiefeng mountain is mainly located in the consequent slope topography with the slope angle 15°~35°

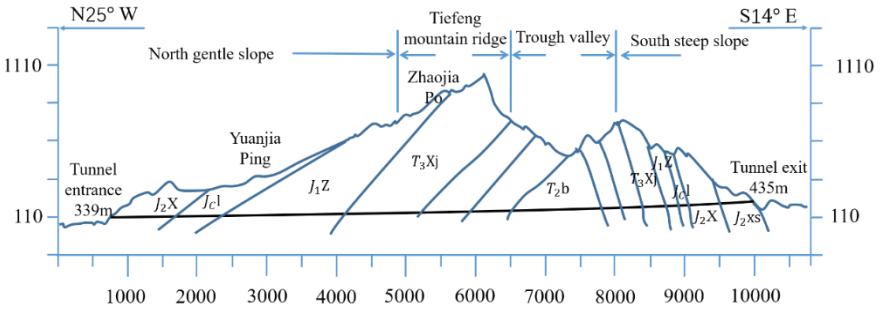

Fig. 13 Geomorphological map of Tiefeng mountain

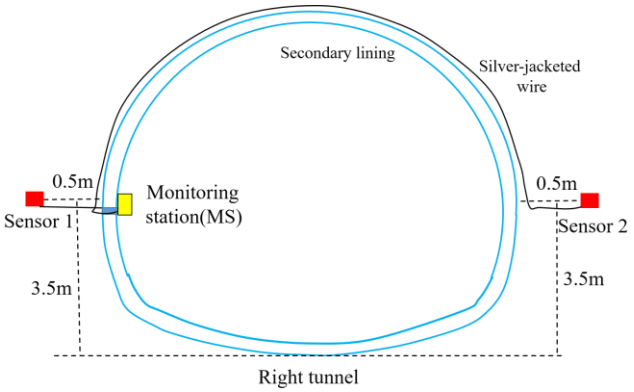

Fig. 14 Schematic diagram of the installed position of sensor

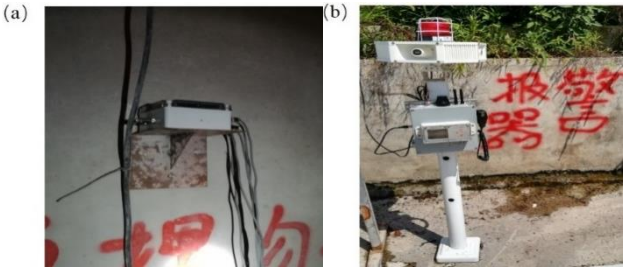

Fig. 15 On-site installed instruments. (a) The MA installation position in the tunnel; and (b) The RCBS installation position outside the tunnel

slightly less than the dip angle of the rock stratum. From the north to the anticline core, the landform is a steep slope which is formed by the Xujiahe formation sandstone. From the north to the south, the topography is the trough valley formed by the mudstone and argillaceous limestone of Badong formation. In the southeast wing of the anticline, the hard sandstone of Xujiahe formation forms a secondary peak with the elevation of 970 m ~ 984 m. In further south, the terrain is cut by gulch, in which the rock mass is also relatively broken, and the terrain slope angle is generally 20°~45°.

During the excavation of the tunnel in Tiefeng mountain, a cross-section of the tunnel was selected for field measurements. According to the engineering information, the liquid metal pressure sensor is installed in the location where the elevation is 630 m and distance is 1200 m from the tunnel exit.

Before the sensor is installed, the boreholes with the depth of 0.5 m perpendicular to the tunnel wall were drilled after the tunnel face is excavated for one hour. Then, the sensor is installed and cement-bentonite is grouted, as shown in Fig. 14. The wires connected to the sensor are long enough to be well connected with the MS after the secondary lining of the tunnel is finished. The MS is installed outside the secondary lining where the sensor is installed, while the RCBS is installed at the sunny location outside the tunnel, as shown in Fig. 15.

4.2 Comparison of numerical results and field measurement data

To further verify the ability of the monitoring system, we compared the measured horizontal stress with the numerical results. In the numerical simulation, it is worth noting that the disturbed domain induced by underground tunnel excavation is generally about twice the diameter of the tunnel. In order to avoid the boundary effect caused by the size of tunnel, the length and height of the numerical model are respectively 147 m and 90 m, as shown in Fig. 16. The material parameters and in-situ stress are shown in Tables 4 and 5. σ_x, σ_y and σ_z represent the horizontal stress, the vertical stress and the longitudinal stress, respectively.

Because of the advantages in treating discontinuous problems and geotechnical engineering problems, the general particle dynamics (GPD) (Zhou *et al.* 2015) is employed to analyze the stress distribution of surrounding rock. In the GPD method, the particles in where tunnels located are removed from the numerical model to simulate the excavation of tunnels. The particle spacing is 0.5 m. Then, the numerical model consists of 7235030 real particles and 745494 virtual particles. In addition, the finite element method (Abaqus) is also used to simulate the deformation of the surrounding rock mass around the tunnels, and the FEM numerical results were basically consistent with the GPD numerical results, as shown in Fig. 17. The numerical results obtained by the two numerical methods and field monitoring data are shown in Table 6. It

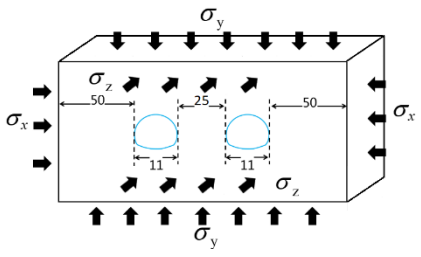

Fig. 16 Cross-section of the numerical model

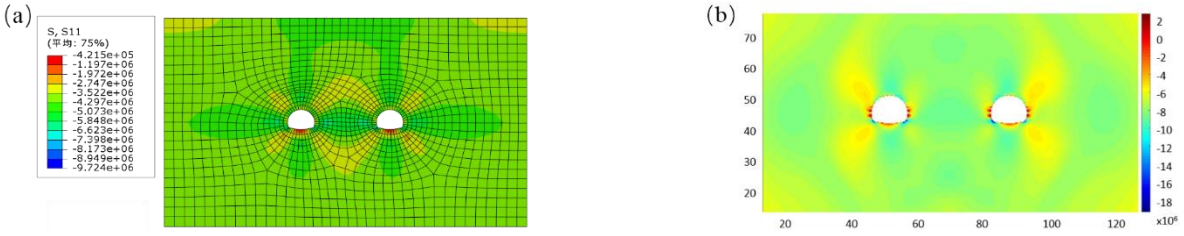

Fig. 17 Horizontal stress contour of tunnel at the monitoring point calculated by Abaqus (a) and GPD method (b)

Table 4 Calculation parameters

Rock classification	Natural density	Elasticity modulus/GPa	Poisson's ratio	Cohesion/MPa	Friction angle/Deg
Marlstone	2650	8.0	0.26	1.0	40

Table 5 The value of in-situ stresses

σ_x (MPa)	σ_y (MPa)	σ_z (MPa)
9	16.7	9.5

Table 6 Comparison of horizontal stress at monitoring points

Method	Stress (MPa)	
GPD	3.255	4.938
ABAQUS	3.567	5.135
Measured (sensor 1)	3.478	---
Measured (sensor 2)	---	4.660

is found from Table 6 that field monitoring data are in good agreement with the numerical results.

5. Conclusions

In this paper, the pressure sensors are mainly improved in size to minimize the disturbance to the in-situ rock-soil, and the measurement range of the sensor is improved to 20 MPa. Moreover, the size of microfluidic channel formed by photolithography technology in PDMS is reduced, and the reliability of the pressure sensors is increased because the smaller the microchannel size, the better the accuracy and sensitivity of the pressure sensor.

The linear relation between resistance change of sensor and pressure is obtained through the calibration test, and the good repeatability of pressure sensor is achieved. Moreover, it is found that the sensor has good stability through comparing the pressure sensor signal output at different loading rates and the test results at fatigue loading. Most important of all, the remote monitoring system composed of liquid metal sensor and remote interactive monitoring device has been successfully applied in the field monitoring, thus the purpose of remote real-time monitoring is realized.

In future work, different types and specifications of sensors are developed to meet the monitoring requirements under different engineering conditions, such as three dimensional liquid metal stress sensor, displacement sensor, and so on.

Acknowledgments

This work was supported by the National Natural Science Foundation of China (Grant Nos. 51839009, 51679017 and 41807251), the Natural Basic Research program 973 of China (Grant No. 2014CB046903), and the Fundamental Research Funds for the Central Universities (Grant No. 2042019kf0037).

References

Ali, M.M. Narakathu, B.B., Emamian, S., Chlaihawi, A.A., Aljanabi, F., Maddipatla, D., Bazuin, B.J. and Atashbar, M.Z. (2016a), "Eutectic Ga-In Liquid Metal Based Flexible Capacitive Pressure Sensor", *Proceedings of the 15th IEEE Sensors Conference*, Orlando, FL, USA, October.

Ali, S., Maddipatla, D., Narakathu, B.B., Chlaihawi, A.A., Emamian, S., Janabi, F., Bazuin, B.J. and Atashbar, M.Z. (2016b), "Flexible Capacitive Pressure Sensor Based on PDMS Substrate and Ga-In Liquid Metal", *Proceedings of the 15th IEEE Sensors Conference*, Orlando, FL, USA, October.

Bakhoum, E.G. and Cheng, M.H.M. (2010a), "Capacitive pressure sensor with very large dynamic range", *IEEE T. Compon. Pack. T.*, **33**(1), 79-83. https://doi.org/10.1109/TCAPT.2009.2022949

Bakhoum, E.G. and Cheng, M.H.M. (2010b), "Novel capacitive pressure sensor", *J. Microelectromech. S.*, **19**(3), 443-450. https://doi.org/10.1109/JMEMS.2010.2047632

Barrias, A., Casas, J.R. and Villalba, S. (2016), "A review of distributed optical fiber sensors for civil engineering applications", *Sensors*, **16**(5), 748. https://doi.org/10.3390/s16050748

Berto, F., Lazzarin, P. and Marangon, C. (2014), "Fatigue strength of notched specimens made of 40CrMoV13.9 under multiaxial loading", *Mater. Des.*, **54**, 57-66. https://doi.org/10.1016/j.matdes.2013.08.013

Chen, W., Gui, X., Liang, B., Yang, R., Zheng, Y., Zhao, C., Li, X., Zhu, H. and Tang, Z. (2017), "Structural Engineering for High Sensitivity, Ultrathin Pressure Sensors Based on Wrinkled Graphene and Anodic Aluminum Oxide Membrane", *ACS Appl. Mater. Interfaces*, **9**(28), 24111-24117. https://doi.org/10.1021/acsami.7b05515

Chossat, J.B., Park, Y.L., Wood, R.J. and Duchaine, V. (2013), "A Soft Strain Sensor Based on Ionic and Metal Liquids", *IEEE Sensors J.*, **13**(9), 3405-3414. https://doi.org/10.1109/JSEN.2013.2263797

Chuang, C.H., Liou, Y.R. and Shieh, M.Y. (2012), "Flexible tactile sensor array for foot pressure mapping system in a biped robot", *Smart Struct. Syst., Int. J.*, **9**(6), 535-547. https://doi.org/10.12989/sss.2012.9.6.535

Cui, Y., Gao, R.X., Yang, D. and Kazmer, D.O. (2007), "A bond graph approach to energy efficiency analysis of a self-powered wireless pressure sensor", *Smart Struct. Syst., Int. J.*, **3**(1), 1-22. https://doi.org/10.12989/sss.2007.3.1.001

Gue, C.Y., Wilcock, M., Alhaddad, M.M., Elshafie, M., Soga, K. and Mair, R. (2014), "Monitoring the effects of tunneling under an existing tunnel-fibre optics", *Proceedings of the 8th International Symposium on Geotechnical Aspects of Underground Construction in Soft Ground*, Seoul, Korea, August. https://doi.org/10.17863/CAM.7210

Haeri, H. and Marji, M.F. (2016), "Simulating the crack propagation and cracks coalescence underneath TBM disc cutters", *Arab. J. Geosci.*, **9**(2), 124. https://doi.org/10.1007/s12517-015-2137-4

Haeri, H., Shahriar, K. and Marji, M.F. (2013), "Simulating the bluntness of TBM disc cutters in rocks using displacement discontinuity method", *Proceedings of the 13th International Conference on Fracture 2013*, Beijing, China, June.

Haeri, H., Tavakoli, H., Shemirani A.B., Sarfarazi, V. and Farazmand, M. (2016), "Evaluating the use of mineral pumice in falling zones of internal pressure tunnels (Case study: Water

transfer tunnel of Sardasht dam power plant)", *J. Min. Sci.*, **52**, 1060-1068. https://doi.org/10.1134/S106273911606160X

Holtz, R.D., Kovacs, W.D. and Sheahan, T.C. (2010), *An Introduction to Geotechnical Engineering*, Pearson, NJ, USA.

Jia, J., Huang, G.T., Deng, J.P. and Pan, K. (2019), "Skin-inspired flexible and high-sensitivity pressure sensors based on rGO films with continuous-gradient wrinkles", *Nanoscale*, **11**, 4258-4266. https://doi.org/10.1039/C8NR08503J

Kim, T., Kim, D.M., Lee, B.J. and Lee, J. (2019), "Soft and Deformable Sensors Based on Liquid Metals", *Sensors*, **19**(9), 4250. https://doi.org/10.3390/s19194250

Klar, A., Levenberg, E., Tur, M. and Zadok, A. (2016), "Sensing for smart infrastructure: Prospective engineering applications", *Proceedings of International Conference on Smart Infrastructure and Construction*, Robinson College, Cambridge, United Kingdom, pp. 289-295. https://doi.org/10.1680/tfitsi.61279.289

Kou, M.M, Liu, X.R., Tang, S.D. and Wang, Y.T. (2019), "3-D X-ray computed tomography on failure characteristics of rock-like materials under coupled hydro-mechanical loading", *Theor. Appl. Fract. Mec.*, **104**, 102396. https://doi.org/10.1016/j.tafmec.2019.102396

Kurtz, A.D., Ned, A.A., Goodman, S. and Epstein, A.H. (2003), "Latest ruggedized high temperature piezoresistive transducers", *NASA Propulsion Measurement Sensor Development Workshop*, Huntsville, Alabama, USA, May.

Kurtz, A.D., Ned, A.A. and Epstein, A.H. (2004), "Improved ruggedized SOI transducers operational above 600°C", *Kulite Semiconductor Products, Inc. Twenty-First Transducer Workshop*, Lexington, Maryland, June.

Li, C., Cordovilla, F. and Ocaña, J.L. (2017), "The design and analysis of a novel structural piezoresistive pressure sensor for low pressure measurement", *Microsys. Technol.*, **23**, 5677-5687. https://doi.org/10.1007/s00542-017-3427-4

Minardo, A., Catalano, E., Coscetta, A., Zeni, G., Zhang, L., Maio, C.D., Vassallo, R., Coviello, R., Macchia, G., Picarelli, L. and Zeni, L. (2018), "Distributed Fiber Optic Sensors for the Monitoring of a Tunnel Crossing a Landslide", Remote Sens., **10**(8), 1291. https://doi.org/10.3390/rs10081291

Nisanth, A., Suja, K.J. and Komaragiri, R. (2014a), "Performance analysis of a silicon piezoresistive pressure sensor based on diaphragm geometry and piezoresistor dimensions", *Proceedings of 2014 IEEE International Conference on Circuits, Power and Computing Technologies* (*ICCPCT*), Nagercoil, India. https://doi.org/10.1109/ICCPCT.2014.7055011

Nisanth, A., Suja, K.J. and Komaragiri, R. (2014b), "Sensitivity enhancement of a silicon based MEMS pressure sensor by optimization of size and position of piezoresistor", *Proceedings of 2014 International Conference on Electronics and Communication Systems* (*ICECS*), Coimbatore, India. https://doi.org/10.1109/ECS.2014.6892720

Oh, J.H., Woo, J.Y., Jo, S. and Han, C.S. (2019), "Pressure-conductive rubber sensor based on liquid-metal-PDMS composite", *Sensor Actuat A-Phys.*, **299**, 111610. https://doi.org/10.1016/j.sna.2019.111610

Orhan, M.H., Dogan, C., Kocaba, H. and Tepehan, G. (2001), "Experimental strain analysis of the high pressure strain gauge pressure transducer and verification by using a finite element method", *Meas. Sci. Technol.*, **12**(3), 335-344. https://doi.org/10.1088/0957-0233/12/3/313

Park, Y.L., Tepayotl-Ramirez, D., Wood, R.J. and Majidi, C. (2012), "Influence of cross-sectional geometry on the sensitivity and hysteresis of liquid-phase electronic pressure sensors", Appl. Phys. Lett., **101**(19), 1097-1104. https://doi.org/10.1063/1.4767217

Raiendra, A., Parmar, B.J., Sharma, A.K., Bhojraj, H., Nayak, M.M. and Rajanna, K. (2005), "Pressure sensor development using hard anodized aluminum diaphragm and sputtered Pt-W thin film strain sensors", *The 13th International Conference on Solid-State Sensors, Actuators and Microsystems*, Seoul, South Korea, Jun. https://doi.org/10.1109/SENSOR.2005.1497327

Ryu, D., Loh, K.J., Ireland, R., Karimzada, M., Yaghmaie, F. and Gusman, A.M. (2011), "In situ reduction of gold nanoparticles in PDMS matrices and applications for large strain sensing", *Smart Struct. Syst., Int. J.*, **8**(5), 471-486. https://doi.org/10.12989/sss.2011.8.5.471

Sarfarazi, V., Haeri, H., Shemirani A.B., Hedayat, A. and Hosseini, S.S. (2017), "Investigation of ratio of TBM disc spacing to penetration depth in rocks with different tensile strengths using PFC2D", *Comput. Concrete, Int. J.*, **20**(4), 429-437. https://doi.org/10.12989/cac.2017.20.4.429

Sarfarazi, V., Haeri, H. and Safavi, S. (2019), "Interaction between two neighboring tunnel using PFC2D", *Struct. Eng. Mech., Int. J.*, **71**(1), 77-87. https://doi.org/10.12989/sem.2019.71.1.077

Signore, M.A., Pascali, C.D., Rescio, G., Taurino, A., Dario, P., Iacovacci, V., Siciliano, P., Martucci, C., Melissano, E., Quaranta, F. and Francioso, L. (2018), "Fabrication and characterization of AlN-based flexible piezoelectric pressure sensor integrated into an artificial pancreas", *Proceedings of the Eurosensors 2018 Conference*, Graz, Austria, **2**(13), 1037. https://doi.org/10.3390/proceedings2131037

Soga, K. and Luo, L.Q. (2018), "Distributed fiber optics sensors for civil engineering infrastructure sensing", *J. Struct. Integr. Maint.*, **3**(1), 1-21. https://doi.org/10.1080/24705314.2018.1426138

Stuchebnikov, V.M. (1991), "SOS strain gauge sensors for force and pressure transducers Sensor", *Actuat. A-Phys.*, **28**(3), 207-213. https://doi.org/10.1016/0924-4247(91)85009-D

Tian, B., Zhao, Y.L., Niu, Z. and Jiang, Z.D. (2014), "Micro-pressure sensor dynamic performance analysis", *Sensor Rev.*, **34**(4), 367-373. https://doi.org/10.1108/SR-11-2013-748

Vorathin, E., Hafizi, Z.M., Ismail, N. and Loman, M. (2020), "Review of high sensitivity fibre-optic pressure sensors for low pressure sensing", *Opt. Laser Technol.*, **121**, 105841. https://doi.org/10.1016/j.optlastec.2019.105841

Wang, X., Gu, Y., Xiong, Z., Cui, Z. and Zhang, T. (2014), "Silk-molded flexible, ultrasensitive, and highly stable electronic skin for monitoring human physiological signals", *Adv. Mater.*, **26**(9), 1336-1342. https://doi.org/10.1002/adma.201304248

Wang, X., Li, H.X., Wang, J. and Wu, A.J. (2019), "A novel fiber-optic pressure sensor device for measuring variceal pressure", *Exp. Ther. Med.*, **18**(6), 4413-4419. https://doi.org/10.3892/etm.2019.8071

Xu, X.M., Soga, K., Nawaz, S., Moss, N., Bowers, K. and Gajia, M. (2015), "Performance monitoring of timber structures in underground construction using wireless SmartPlank", *Smart Struct. Syst., Int. J.*, **15**(3), 769-785. https://doi.org/10.12989/sss.2015.15.3.769

Yan, J.W., Zhou, J.C., Lu, S.Q. and Tian, L. (2005), "Development and investigation trends of alloy thin film piezoresistive sensor", *Mater. Rev.*, **19**(12), 31-34. https://doi.org/10.3321/j.issn:1005-023X.2005.12.009

Yu, H.Y. and Huang, J.Q. (2015), "Design and Application of a High Sensitivity Piezoresistive Pressure Sensor for Low Pressure Conditions", *Sensors*, **15**(9), 22692-22704. https://doi.org/10.3390/s150922692

Yu, H.Y., Qin, M. and Huang, J.Q. (2013), "A piezoresistive pressure sensor with improved sensitivity in low pressure condition", *Proceedings of the 12th IEEE Sensors Conference*, Baltimore, MD, USA, November. https://doi.org/10.1109/ICSENS.2013.6688390

Zhang, S.R., Wen, B. and Cui, G.H. (2001), "A kind of SOS high temperature pressure transducer with double membrane", *Journal of Natural Science of Heilongjiang University*, **18**(4),

56-58. http://dx.chinadoi.cn/10.3969/j.issn.1001-7011.2001.04.013

Zhang, Y., Hu, Y.G., Zhu, P.L., Han, F., Zhu, Y., Sun, R. and Wong, C.P. (2017), "Flexible and Highly Sensitive Pressure Sensor Based on Microdome-Patterned PDMS Forming with Assistance of Colloid Self-Assembly and Replica Technique for Wearable Electronics", *ACS Appl. Mater. Interfaces*, **9**(41), 35968-35976. https://doi.org/10.1021/acsami.7b09617

Zhang, X.Y., Hu, Y.G., Gu, H., Zhu, P., Jiang, W.L., Zhang, G., Sun, R. and Wong, C.P. (2019), "A Highly Sensitive and Cost-Eective Flexible Pressure Sensor with Micropillar Arrays Fabricated by Novel Metal-Assisted Chemical Etching for Wearable Electronics", *Adv. Mater. Technol.*, **4**(9), 1900367. https://doi.org/10.1002/admt.201900367

Zhao, Y.L., Zhao, L.B. and Jiang, Z.D. (2006), "High temperature and frequency pressure sensor based on silicon-on-insulator layers", *Meas. Sci. Technol.*, **17**(3), 519-523. https://doi.org/10.1088/0957-0233/17/3/S11

Zhao, L.B., Guo, X., Meng, X.W., Hebibul, R., Zhao, Y.L., Wang, J.Z. and Jiang, Z.D. (2013), "An ultra-high pressure sensor with cylinder structure", *J. Mech. Sci. Technol.*, **27**(8), 2383-2389. https://doi.org/10.1007/s12206-013-0623-8

Zhou, X.P., Bi, J. and Qian, Q.H. (2015), "Numerical simulation of crack growth and coalescence in rock-like materials containing multiple pre-existing flaws", *Rock Mech. Rock Eng.*, **48**, 1097-1114. https://doi.org/10.1007/s00603-014-0627-4

Zhou, X.P., Deng, R.S. and Zhu, J.Y. (2018), "Three-layer-stacked pressure sensor with a liquid metal-embedded elastomer", *J. Micromech. Microeng.*, **28**(8), 085020. https://doi.org/10.1088/1361-6439/aac13c

Zhou, X.P., He, Y. and Zeng, J. (2019), "Liquid metal antenna-based pressure sensor", *Smart Mater. Struct.*, **28**(2), 025019. https://doi.org/10.1088/1361-665X/aaf842.

BS